ESEM study of the humidity-induced swelling of clay film

Benoît Carrier, Linlin Wang, Matthieu Vandamme, Roland Pellenq, Michel Bornert, Arnaud Tanguy, Henri van Damme

ESEM Study of the Humidity-Induced Swelling of Clay Film

Benoit Carrier,† Linlin Wang,‡ Matthieu Vandamme,*,† Roland J.-M. Pellenq,§,∥,⊥ Michel Bornert,† Alexandre Tanguy,‡ and Henri Van Damme#

†Laboratoire Navier (UMR 8205), CNRS, ENPC, IFSTTAR, Université Paris-Est, F-77455 Marne-la-Vallée, France
‡Laboratoire de Me canique des Solides, CNRS UMR 7649, Ecole Polytechnique, 91128 Palaiseau, Cedex, France
§Department of Civil and Environmental Engineering, Massachusetts Institute of Technology, 77 Massachusetts Avenue, Cambridge, Massachusetts 02139, United States
∥Centre Interdisciplinaire des Nanosciences de Marseille, CNRS (UPR 7251), Campus de Luminy, 13288 Marseille Cedex 09, France
⊥<MSE > 2, UMI 3466, CNRS-MIT, 77 Massachusetts Avenue, Cambridge, Massachusetts 02139, United States
#Université Paris-Est, IFSTTAR, Marne-la-Vallée, France

ABSTRACT: We measured the humidity-induced swelling of thin self-standing films of montmorillonite clay by a combination of environmental scanning electron microscopy (ESEM) and digital image correlation (DIC). The films were about 40 μm thick. They were prepared by depositing and evaporating a suspension of clay and peeling off the highly oriented deposits. The rationale for creating such original samples was to obtain mesoscopic samples that could be used to bridge experimentally the gap between the scale of the clay layer and the engineering scale of a macroscopic clay sample. Several montmorillonite samples were used: the reference clay Swy-2, the same clay homoionized with sodium or calcium ions, and a sodium-exchanged Cloisite. The edges of the clay films were observed by ESEM at various relative humidity values between 14% and 95%. The ESEM images were then analyzed by DIC to measure the swelling or the shrinkage of the films. We also measured the adsorption/desorption isotherms by weighing the film samples in a humidity-controlled environment. In order to analyze our results, we compared our swelling/shrinkage and adsorption/desorption data with previously published data on the interlayer spacing obtained by X-ray diffraction and with numerical estimates of the interlayer water obtained by molecular dynamics simulation. The swelling and the hysteresis of this swelling were found to be comparable for the overall macroscopic films and for the interlayer space. The same correspondence between film and interlayer space was observed for the amount of adsorbed water. This suggests that, in the range of relative humidities values explored, the films behave like freely swelling oriented stacks of clay layers, without any significant contribution from the mesoporosity. The relevance of this result for the behavior of clayey sedimentary rocks and the differences with the behavior of nonoriented samples (powders or compacted powders) are briefly discussed.

1. INTRODUCTION

Swelling clays have the property to expand significantly in the presence of water. The understanding and quantifying of this swelling behavior have critical safety and economical consequences for many industrial applications. In civil engineering, the shrinkage and swelling of clays have huge repercussions on the stability of soils and building foundations. Forty years ago the annual cost of damages to buildings caused by clay swelling in the US was estimated at 2.3 billion US dollars.[1] In the petroleum industry, this swelling has important implications for drilling operations: in contact with the aqueous drilling fluids, clay swells, which can lead to well-bore instability.[2] Swelling clays are also considered as potential engineered barriers for nuclear waste disposal.[3] For this latter application, swelling is expected to be beneficial, as it will enable to fill the gap between the bentonite plug and the argillite rock during resaturation of the plug and thus will decrease the permeability of the barrier.

Several methods are commonly used to measure the swelling of clays, from X-ray diffraction (XRD) experiments at the nanoscale[4] to macroscale geotechnical tests (oedometer test, macroscopic free swelling test, etc.).[3,5] However, clay materials exhibit complex multiscale structure and pore network. Therefore, determining the sequence of mechanisms that lead to hydration and swelling upon imbibition is a challenge.[6]

This work focuses on the swelling of montmorillonite clay. Montmorillonite is a clay mineral member of the smectite family. Its basic structure is made of negatively charged layers.

Each layer consists of one octahedral sheet between two tetrahedral sheets and is less than 1 nm thick. The layers bear a net negative charge because of atom substitutions in the crystalline structure. This negative charge is balanced by interlayer cations, Na^+ and Ca^{2+} being the most common. The interlayer space also contains water molecules in various amounts. The clay layers are stacked to form ordered structures called "particles" separated by mesopores. The thickness of the particles depends on the charge and size of the cation and on the charge of the layer.[7−10] In natural clays, the clustering of these particles forms "aggregates". The size of theses aggregates typically ranges from 1 to 10 μm.

At the smaller scale, the interlayer spacing can be measured by XRD. The evolution of the basal spacing of montmorillonite with relative humidity has been studied for decades with such a technique.[4,11−13] These experiments highlighted two swelling regimes: a short-range crystalline swelling and an osmotic swelling at greater basal spacings. XRD patterns and molecular simulations[14−16] showed that the basal spacing increases with water content in a discrete fashion with the intercalation of 0, 1, 2, or 3 planes of water molecules during the crystalline swelling. Bérend et al.[11] and Cases et al.[12] investigated the influence of the interlayer cation on the crystalline swelling and on the adsorption isotherms. They observed a great impact of the size and charge of the cation on the magnitude of the swelling and the quantity of adsorbed water. Ferrage et al.[13] measured the basal spacing of monoionic montmorillonite samples with various counterions for relative humidities ranging from 0% to 80%. Consistently with previous works, they observed structures with 0, 1, and 2 layers of interlayer water. However, they showed that the swelling of the interlayer space is not homogeneous in the sample.

Thermoporometry in unsaturated porous medium[6] makes it possible to measure the evolution of the size of the mesopores at various relative humidities. The nature of the interlayer cation strongly influences the swelling of the mesopores. For some cations (i.e., Na^+, Li^+) the swelling of the mesopores occurs before the complete filling of the interlayer space. In contrast, the mesopores do not swell with other cations (i.e., K^+, Cs^+, Ca^{2+}). The swelling of the mesopores is shown to be due to an osmotic swelling.

Recently, environmental scanning electron microscopy (ESEM) made it possible to observe clay materials at the microscale under controlled environmental conditions.[17] Montes-H et al.[18−20] used ESEM and digital image analysis to investigate the swelling/shrinkage of bentonite—a montmorillonite-rich clay. They measured the swelling of about 50 μm wide aggregates at relative humidities ranging from 10% to 80%. They investigated the influence of the interlayer cation and of the compaction. Adsorption isotherms and swelling depend strongly on the interlayer cation.[19] For instance, Na^+-bentonite swells more than Ca^{2+}-bentonite. Although raw bentonite contains more Na^+ than Ca^{2+}, it behaves like a Ca^{2+}-bentonite. Maison[21] developed a microweighing device to weigh clay aggregates in an ESEM chamber. The swellings of clays from various natural clay deposits were observed and directly related to the clay water content. Wang et al.[22−24] observed the swelling behavior of an argillite in an ESEM chamber. They used digital image correlation (DIC)[25] to measure the strain field upon hydration: the deformations in the argillite are very heterogeneous and irreversible deformations are observed. However, understanding the links between the swelling at various scales remains a challenging task.

In this work we used ESEM to observe the swelling/shrinkage of thin films of montmorillonite clay. Although the humidity-induced swelling of clays at the scale of the layer (i.e., the nanometer) on one hand and at the scale of the engineer on the other hand is well characterized, either by XRD experiments or by macroscopic testing, respectively, filling the gap between these scales is a very challenging work. Clay materials exhibit indeed a complex multiscale structure with a multiscale porosity. The links between the swelling of the interlayer space and the macroscopic swelling are not yet fully understood. Working on model mesoscopic clay samples aimed at filling this gap and at showing how the swelling of the interlayer space impacts the swelling at the mesoscopic scale. The objectives of this work are to investigate the effect of the valency of the interlayer cation on the swelling of a well-ordered clay-based structure and to better understand the swelling mechanisms of smectite clays.

We prepared thin self-standing films of montmorillonite as suggested by Zabat[26] in order to work on a well-ordered system with nearly parallel clay platelets. We observed the edge of these films with an ESEM at a controlled relative humidity. We then used DIC techniques on the high-resolution ESEM images to measure the swelling/shrinkage of the films. In another setup, we also measured the adsorption isotherms of the films, i.e., the exact quantity of water in the film at a given relative humidity.

The interest of this work lies in the fact that the swelling was measured on a well-ordered system made of nearly parallel clay platelets. In particular, we investigated the influence of the interlayer cation on the swelling behavior. Working on thin clay films provides a deeper insight into the swelling mechanisms at the mesoscale and into the interplay between mechanisms at micro- and mesoscales.

2. MATERIALS AND METHODS

We used four types of materials: the reference Wyoming montmorillonite Swy-2 (coined raw-Swy-2), the Swy-2 homoionized with sodium (coined Na^+-Swy-2), the Swy-2 homoionized with calcium (coined Ca^{2+}-Swy-2), and the Wyoming montmorillonite Cloisite homoionized with sodium (coined Na^+-Cloisite). With those materials, we prepared self-standing clay films. On all films, we measured the water adsorption isotherms (see section 2.4). On the films made with raw-Swy-2, Ca^{2+}-Swy-2, and Na^+-Cloisite, we measured the humidity-induced swelling by using a combination of ESEM characterization (see section 2.2) and DIC (see section 2.3).

2.1. Sample Preparation. The first smectite clay used in this work is the reference Wyoming montmorillonite Swy-2 purchased from the Source Clay Repository of the Clay Mineral Society.[27] The structural formula of the Swy-2[28] is $(Al_{3.23}Mg_{0.56}Fe_{0.42})(Si_{7.89}Al_{0.11})O_{20}(OH)_4(Ca_{0.16}Na_{0.36}K_{0.03})$. Thus, the initial relative proportions of the sodium cations and of the calcium cations were about 2/3 and 1/3, respectively. First, the clay fraction with particles smaller than 2 μm was isolated by following the process described by Arroyo et al.[29] Then the clay was homoionized and deposited in thin films, as described next.

To isolate the particles smaller than 2 μm, the clay Swy-2 was first suspended in 300 mL of water. The suspension was then stirred using a magnetic stir bar for 48 h and centrifuged for 5 min at 2000*g* (where *g* is the acceleration of gravity). The supernatant solution was collected while the deposit was dispersed in 300 mL of water and centrifuged for 3 min at 2000*g*. The supernatant solution was collected and added to the supernatant already collected. The clay suspension was centrifuged for 15 min at 3000*g* and the supernatant discarded. One-third of the clay fraction was suspended again in water to prepare the natural clay samples raw-Swy-2. The other two-thirds were saturated with sodium

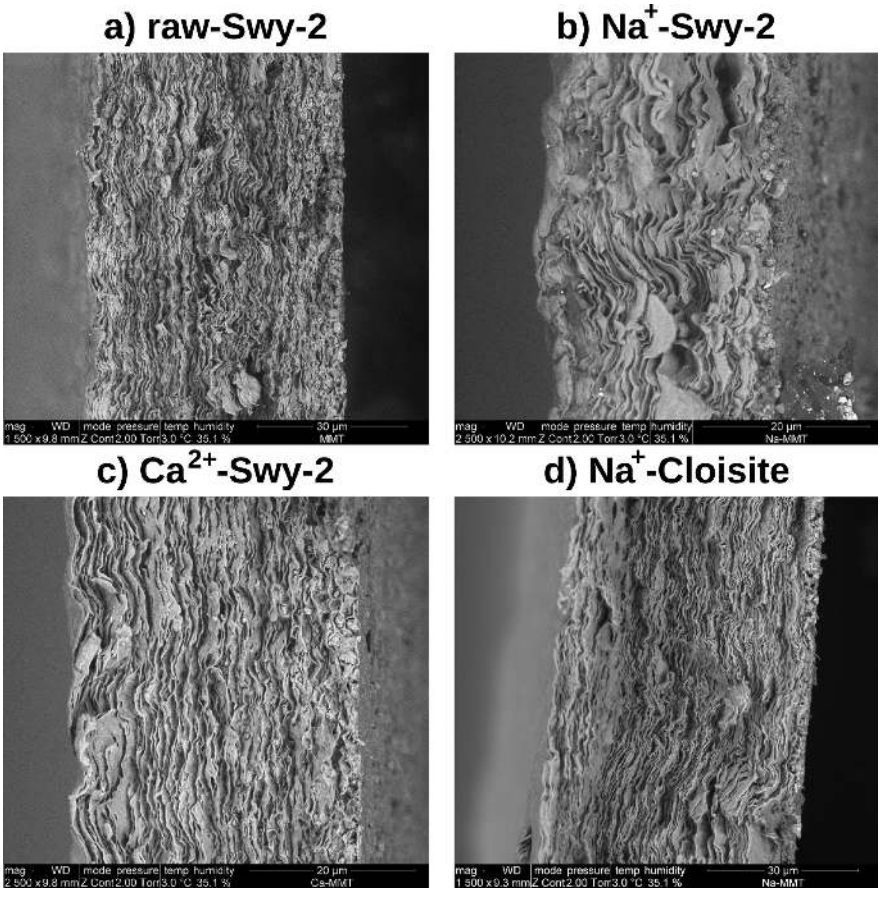

Figure 1. ESEM observation at a relative humidity of 35% of the edges of (a) a raw-Swy-2 film, (b) a Na^+-Swy-2 film, (c) a Ca^{2+}-Swy-2 film, and (d) a Na^+-Cloisite film.

or calcium cations to prepare the Na^+-Swy-2 and Ca^{2+}-Swy-2 samples, respectively.

To obtain homoionic samples, the clay was treated with concentrated solutions of sodium or calcium chloride. The clay fraction was dispersed into 250 mL of 1 N salt solution. The solution was stirred for 24 h and centrifuged at 4000*g* for 10 min. The supernatant was discarded. This process was repeated four times. The cation-saturated clay was then washed with water to remove chloride anions. The clay was suspended in 300 mL of water. The solution was put in a porous membrane tubing and dialyzed in 2 L of water. The water was stirred and changed every 24 h until the silver nitrate test for chloride ions became negative. A clay suspension of concentration around 7 g/L was then obtained.

The clay suspension was deposited on a flat polyethylene surface to prepare thin films of oriented clay grains. After a 72 h long drying at room temperature and relative humidity, a solid thin film could be peeled off from the polyethylene surface. Depending on the quantity of clay in the system and on the water content, the thicknesses of the films were between 30 and 60 μm and the surface density of the dry films lay between 3 and 6 mg/cm^2.

We also used a Na^+-Cloisite (i.e., a Cloisite monoionized with sodium cations) purchased from Southern Clay Products to prepare thin films. Cloisite is another purified natural low-charge Wyoming montmorillonite with an extremely limited number of tetrahedral substitutions. Cloisite and Swy-2 have the same layer charge of about 0.7 per unit cell. The structural formula of the Na^+-Cloisite[30] $(Al_{2.90}Mg_{0.59}Fe_{0.49}Ti_{0.01})(Si_{7.92}Al_{0.08})O_{20}(OH)_4Na_{0.70}$ is very close to the structural formula of the Swy-2.

To check the validity of the cation exchange protocol, the chemical composition of the samples was analyzed by X-ray energy dispersive spectroscopy (EDS) after carbon-coating. In the natural Swy-2 sample, both sodium and calcium cations were detected. In the Na^+-Swy-2 and Ca^{2+}-Swy-2 samples, only sodium cations or calcium cations, respectively, were detected, while chloride anions were undetectable. In the Na^+-Cloisite sample, only sodium cations were detected.

2.2. ESEM Observation. The edges of the clay films were observed by environmental scanning electron microscopy (ESEM). We used a FEI Quanta 600 microscope. Acquisition was performed perpendicular to the edge of the sample. We broke the films to expose their edge. We did not use a blade to cut the films because they would have been crushed. One side of a few millimeters wide sample was then glued vertically on a small copper piece with a heat conducting adhesive. The upper half-millimeter of the film jutted out the adhesive and the copper, so that the deformations were free in the zone observed by the ESEM. Figure 1 displays examples of an acquisition on each type of sample. For the raw-Swy-2, Ca^{2+}-Swy-2, and Na^+-Cloisite samples, the particles were deposited almost in very good parallel arrangement. In contrast, we did not succeed in obtaining Na^+-Swy-2 films with an ordered enough structure; therefore, the Na^+-Swy-2 samples were not used for humidity-induced swelling characterization.

During observation, the temperature of the samples was controlled with a Peltier cooling system. All observations were carried out at a constant sample temperature of 3 °C. The relative humidity was controlled by changing the water vapor pressure in the chamber, as shown in Table 1.

The clay sample was dried or hydrated step by step. The samples were very thin, and therefore their equilibration was quick, around 30 min. To ensure that equilibrium was reached, two images of the samples were taken at 5 min intervals, and we checked that no deformation could be detected between the two states. At each step and after equilibration, high-resolution images of several regions of the sample were taken. The images were obtained by using a backscattered electron detector. In this work, we acquired 4096 × 3775 pixel ESEM

Table 1. Vapor Pressure in the ESEM Chamber and Corresponding Relative Humidity[a]

chamber pressure (Torr)	chamber pressure (Pa)	relative humidity (%)
0.80	107	14.1
2.00	267	35.1
3.13	417	55.0
4.30	573	75.5
5.40	720	94.8

[a]The temperature of the sample was kept constant (3 °C) during all tests.

images at a magnification of 1500 or 2500. Therefore, the physical size of a pixel was 20 and 12.5 nm, respectively.

For each material (i.e., raw-Swy-2, Ca^{2+}-Swy-2, Na^{+}-Cloisite), two different samples were observed at one or two different locations along the edge of the film. For the first sample of each material, the following sequence of increasing relative humidities (RH) was applied: 35.1%, 55.0%, 75.5%, 94.8%. For the second sample, the following sequence of relative humidities was applied: 35.1%, 75.5%, 35.1%, 75.5%, 94.8%, 75.5%, 35.1%, 14.1%, 94.8%, 35.1%. Before each sequence, a partial vacuum was applied to the chamber of the ESEM to replace the air with water vapor. Therefore, the initial state at a relative humidity of 35.1% was reached by adsorption.

For each image, the swelling of the film was inferred by using digital image correlation techniques, as explained in the next section.

2.3. Digital Image Correlation Technique. Digital image correlation (DIC) is a contact-free technique used to measure the deformation of samples between a reference image and an image of the deformed state.[25] DIC was recently applied to analyze ESEM images.[22−24,31] DIC compares the gray levels of two images acquired by the electron microscope and computes the displacement field that transports material points from the reference image into the deformed image. Deformations can then be computed from the displacement field by the method proposed by Allais et al.[32] The displacement gradient was computed by a contour integral. Then, the linear strain tensor was obtained by taking the symmetric part of the displacement gradient. The axes of the strain tensor were chosen as the axes of the image. In the following sections, the transversal strain is the component of the strain tensor orthogonal to the clay film, i.e., the out-of-plane component with regard to the plane of the film, and the longitudinal strain is the component of the strain tensor parallel to the film, i.e., the in-plane component. In a given direction, the strain we computed is the engineering strain ε, which is defined by

$$\varepsilon = \frac{l}{L} - 1 \tag{1}$$

where L and l are the lengths of an object in the reference state and in the deformed state, respectively.

By choosing contours of various sizes to compute the displacement gradient by the method of Allais et al.,[32] the strain can be measured at various scales. Although DIC makes it possible to characterize deformations locally and to compute the strain field on each point of the grid, in this study we only used this technique to characterize the global deformation of the area of interest. Indeed, we could obtain no significant information from the analysis of the local strain field. The particles which jut out the sample can bend because of their flexibility and induce an apparent deformation which is independent from the homogeneous deformation.

In this work, we used ESEM images of the edge of the clay films, acquired at a magnification of 1500 or 2500 depending on the amplitude of the swelling. The gray levels were encoded on 8 bits. The images were processed with the in-house software CMV.[33] The size of the correlation window was 50 × 50 pixels for a magnification of 1500 and 80 × 80 pixels for a magnification of 2500. In both cases, the physical size of the correlation window was 1 μm^2. Indeed, the contrast is sufficient at this scale for DIC, with about two separate clay particles in a correlation window.

On each ESEM image, the average strain was measured by DIC on two zones of various sizes (Figure 2): a large zone (in blue in Figure 2)

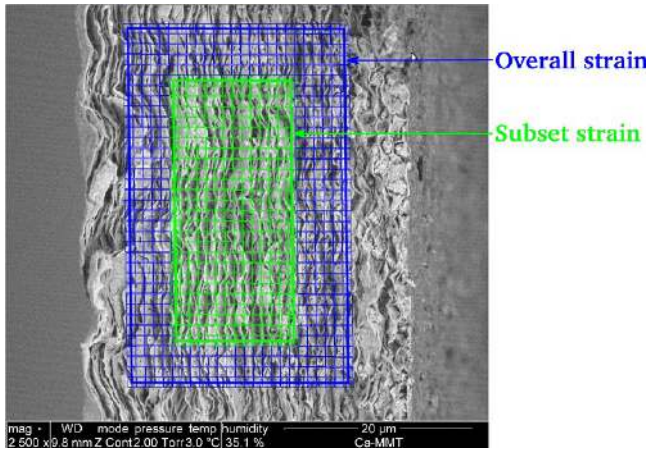

Figure 2. Measurement of the swelling strain of a Ca^{2+}-Swy-2 sample on two zones of different sizes. The small squares around each point of the grid are the correlation windows, i.e., the zones on which gray levels were compared between the reference and the deformed images to compute the displacement of the point at the center of the window.

and a smaller zone (in green in Figure 2). Performing DIC on two zones with different sizes aimed at verifying whether the size of the zone of interest had an influence on the measured strain. The error of the strain measurement by DIC originates in several phenomena: image noise, evolution of the contrast, image-processing parameters.[34] However, in this work we considered only the average strain on large zones for which these measurement errors are negligible.

2.4. Water Sorption Isotherms. The water sorption isotherms were obtained on the four types of samples prepared (i.e., raw-Swy-2, Na^{+}-Swy-2, Ca^{2+}-Swy-2, Na^{+}-Cloisite) by weighing the samples in a desiccation chamber. The relative humidity was controlled in the chamber with saturated salt solutions. Air was first blown into a saturated salt solution to bring it to the desired moisture and then into the chamber. The relative humidity was recorded with a capacitive hygrometer (with an accuracy of 1%). The chamber was kept at room temperature (20 °C). After each change of the imposed relative humidity, the sample was weighed after equilibration, considered to be reached when the relative mass of the sample varied less than 0.1% over 10 min. The mass of the dry clay was measured after a 4 h long drying at 110 °C.

3. RESULTS

3.1. Swelling and Shrinkage. Figure 3 shows the edge of a film of Ca^{2+}-Swy-2 observed by ESEM at some of the various relative humidities considered. At each increase of humidity, a significant swelling orthogonal to the film can be observed with the naked eye.

The transversal strain and the longitudinal strain of all samples are displayed in Figure 4 upon hydration only. First, one observes that the amplitude of the swelling was strongly dependent on the interlayer cation. Second, as expected, the strain response to hydration was very anisotropic. The longitudinal strain was more than 1 order of magnitude smaller than the transversal strain. However, the longitudinal strain was not equal to zero and increased slightly with relative humidity, all the more so as the transversal strain was large. This correlation between the longitudinal and the transversal strains suggests that the small longitudinal swelling was due to the spatial oscillations and misalignment of the clay particles which are not perfectly parallel to the mean plane of the film.

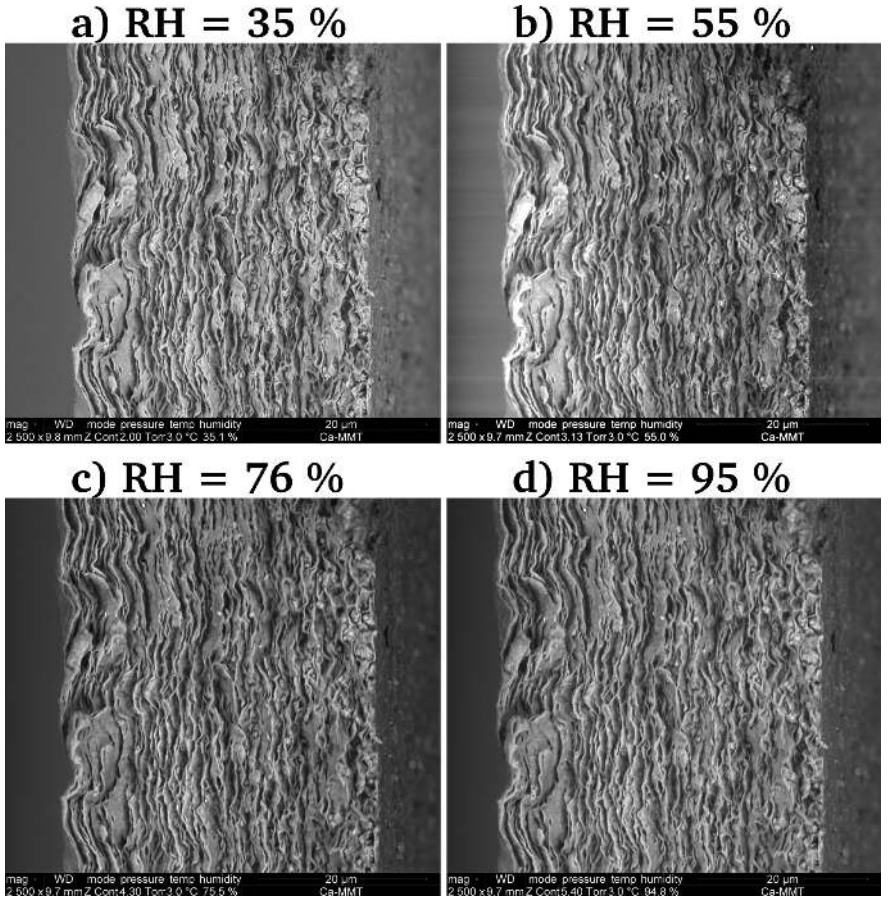

Figure 3. ESEM observation of the edge of a Ca^{2+}-Swy-2 film at various relative humidities (RH).

In order to validate the reproducibility of our measurements and to estimate the uncertainty of the method, we performed swelling measurements for each material on two different samples. On each film, one or two locations, far from each other, were analyzed. Moreover, on each location, the strain was measured on two zones of different sizes. The average transversal swelling between RH = 35% and 95% for raw-Swy-2 was 27.5 ± 2.5%, for Ca^{2+}-Swy-2 was 13.7 ± 2.3%, and for Na^{+}-Cloisite was 40.3 ± 3.3%. The relative fluctuation for the transversal swelling was around 8% for raw-Swy-2 and Na^{+}-Cloisite at all relative humidities. For Ca^{2+}-Swy-2 the relative error was around 13%, as a consequence of its smaller swelling. From those low relative errors, we concluded that our measurements were reproducible and meaningful. The observed uncertainty did not originate in the error in the DIC method, which is negligible at this scale. A potential source of error stemmed from the fact that the sample was not perfectly vertical. For instance, in Figure 1a, the top of the film is visible on the left, while in Figure 1c, the bottom of the film is visible on the right. In both cases, the films exhibited a small angle α with the vertical axis. The relative error that this tilt induces on the transversal strain measurement was equal to $\alpha^2/2$. For $\alpha = 10°$ and 20°, the relative errors were equal to 1.5% and 6.1%, respectively, which are smaller than the measured relative errors. Therefore, the observed uncertainties must have originated partly in the natural fluctuations of the structures and properties of the samples. Moreover, the strain did not depend on the size of the measurement zone. The deformation was homogeneous at this scale. Therefore, the green zone, which was about 10 μm wide, is a representative elementary volume of the material. However, at a finer scale this homogeneity disappeared.

For samples raw-Swy-2, Ca^{2+}-Swy-2, and Na^{+}-Cloisite, Figure 5 displays the swelling when relative humidity was increased from 35% to 95% and the shrinkage when relative humidity was subsequently decreased from 95% to 14%. The displayed data are the overall strains measured on one location of one sample, on which a complete hydration−dehydration cycle was performed. These data correspond to the empty triangles pointing down in Figure 4.

The sample Ca^{2+}-Swy-2 swelled less than the other two samples for relative humidities above 35%. However, this same sample deformed more than the other two at relative humidities below 35%. A shrinkage of more than 8% was observed for Ca^{2+}-Swy-2 between relative humidities of 35% and 14%, while raw-Swy-2 and Na^{+}-Cloisite shrinked by 4% only. For relative humidities below 75%, raw-Swy-2 and Na^{+}-Cloisite exhibited similar swellings or shrinkages. For relative humidities above 75%, Na^{+}-Cloisite swelled significantly more than raw-Swy-2. For all samples, an hysteresis could be observed upon hydration and dehydration.

Figures 6a−c display the swellings of all films during two successive hydration/dehydration cycles. Except for the very first hydration step for the sample raw-Swy-2, no irreversible deformation was observed. Figures 6d−f show the humidity-induced strains in function of the quantity of adsorbed water. These data were obtained from the combination of the swelling measurements displayed in Figures 6a−c with the adsorption isotherms displayed in Figure 7. The swellings in function of

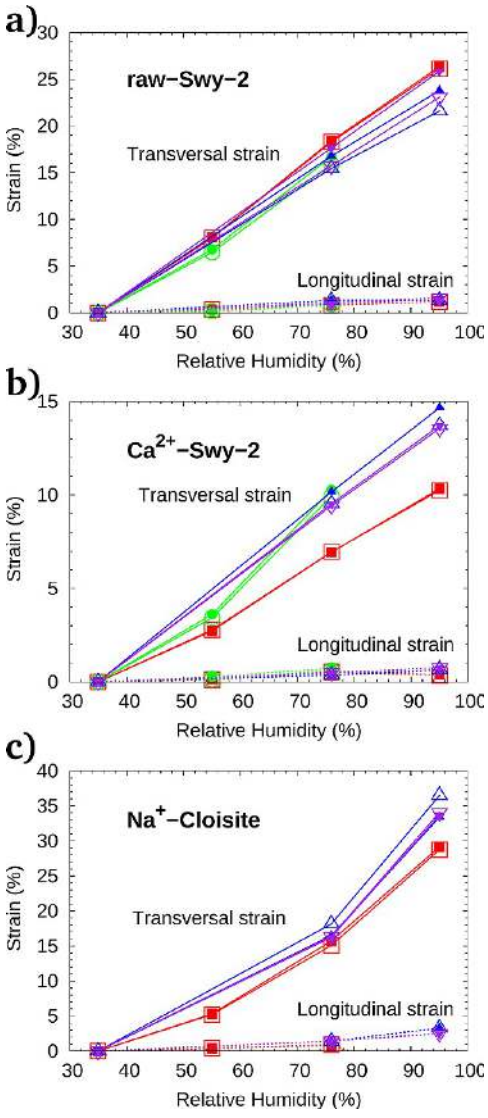

Figure 4. Transversal (solid lines) and longitudinal (dashed lines) strains of clay films: (a) raw-Swy-2, (b) Ca^{2+}-Swy-2, (c) Na^{+}-Cloisite. Each color or symbol shape corresponds to a different measurement. For each material, two different films were observed, and on each film one or two independent locations were analyzed. The transversal strain is the component of the strain tensor orthogonal to the film, while the longitudinal strain is the component parallel to the film. The strains were measured for each sample on two zones (see Figure 2): a large zone (open symbols) and a smaller subset of this zone (plain symbols).

the amounts of water adsorbed in the films were well-approximated by a linear relationship.

3.2. Sorption−Desorption Isotherms. Figure 7 displays the sorption−desorption isotherms at 20 °C for all montmorillonite samples. The experimental sorption isotherms were fitted with the D'Arcy−Watt equation:[35]

$$w = \frac{abr_H}{1 + br_H} + cr_H + \frac{\alpha\beta r_H}{1 - \beta r_H} \quad (2)$$

where w is the water content, r_H the relative humidity, and a, b, c, α, and β are the fitted parameters. No quantitative analysis of the parameters was possible. The fitting was performed only to capture the trend of the isotherms and to provide a guide for the eye.

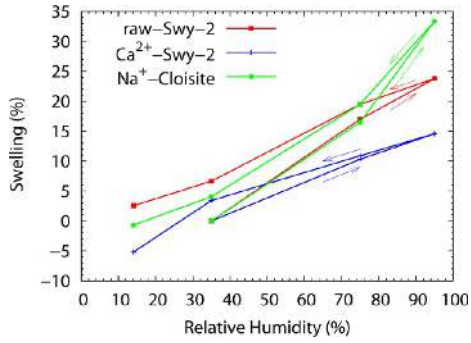

Figure 5. Swelling and shrinkage measured by ESEM and digital image correlation for three montmorillonite samples. The initial state at a relative humidity of 35% was chosen as the reference state.

The amount of water adsorbed at a relative humidity of 90% was roughly the same for all samples and was comprised between 0.24 and 0.25 g/g of dry clay. However, the shape of the isotherms varied significantly with the samples. The isotherm of the Ca^{2+}-saturated sample Ca^{2+}-Swy-2 (Figure 7c) showed a high potential for water adsorption between RH = 0% and 40% and a low potential for water adsorption between RH = 40% and 90%. In contrast, the adsorption isotherms of the Na^{+}-saturated samples Na^{+}-Swy-2 and Na^{+}-Cloisite exhibited opposite convexity and a high potential for water adsorption at high relative humidities. The amplitude of the hysteresis differed depending on the interlayer cation. Indeed, while the amplitude of the hysteresis was very limited (∼12 mg/g at RH = 45%) for the Ca^{2+}-saturated Ca^{2+}-Swy-2 sample, this hysteresis was much higher (∼44 mg/g at RH = 45%) for the Na^{+}-saturated samples Na^{+}-Swy-2 and Na^{+}-Cloisite. The natural montmorillonite raw-Swy-2—which contained both Na^{+} and Ca^{2+}—exhibited the same adsorption behavior as the Na^{+}-saturated samples, in terms of both convexity of the adsorption isotherm and the amplitude of the hysteresis.

4. DISCUSSION

Clay swelling is governed by two mechanisms: a crystalline interlayer swelling and an interparticle osmotic swelling. In order to determine the origin of the swelling of the clay films, we compared our data on the swelling and the quantity of adsorbed water in the films with available data on the hydration of the interlayer space. We will thus show that the clay films exhibit no osmotic swelling.

4.1. Comparison with Available Data on Swelling. Figure 1 of the Supporting Information displays the results of the XRD experiments on montmorillonite of Bérend et al.[11] and Cases et al.[12] Their data are the only ones which we are aware of that cover a complete cycle of adsorption/desorption. The Wyoming montmorillonite used by Bérend et al.[11] and Cases et al.[12] had a structural formula very similar to that of the Swy-2 montmorillonite used in our study.

The interlayer spaces of the Na^{+}-saturated montmorillonite and the Ca^{2+}-saturated montmorillonite (see Supporting Information) exhibited a very different swelling. The Na^{+}-saturated montmorillonite started forming the first layer of water at RH = 20% and the second at RH = 60% while the Ca^{2+}-saturated montmorillonite formed two layers of water at relative humidities below 40%. Figure 1 of the Supporting Information also displays the typical values of the interlayer spacing for the dehydrated, monohydrated, and bihydrated

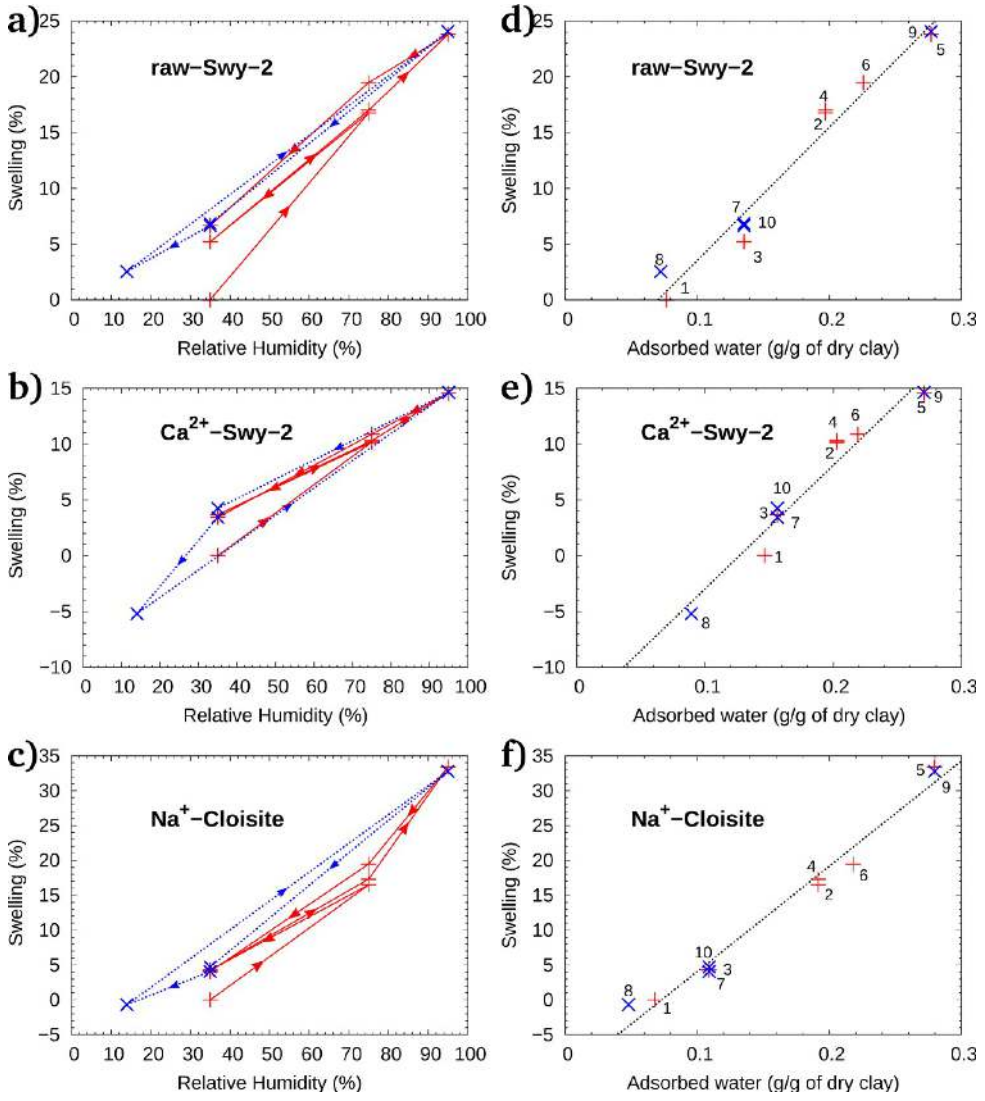

Figure 6. Swelling and shrinkage measured by ESEM and digital image correlation in function of the relative humidity (left). The first hydration/dehydration cycle is displayed in red (solid line) while the second hydration/dehydration cycle is displayed in blue (dashed line). (a) raw-Swy-2, (b) Ca^{2+}-Swy-2, and (c) Na^{+}-Cloisite. Swelling and shrinkage in function of the amount of water adsorbed: (d) raw-Swy-2, (e) Ca^{2+}-Swy-2, and (f) Na^{+}-Cloisite. Straight crosses correspond to the first hydration/dehydration cycle, while tipped crosses correspond to the second hydration/dehydration cycle. The black dashed-line is a linear fit of the displayed data. The numbers on the plots of the right column are the orders of the experiments.

montmorillonite: many data points lie outside these well delimited discrete hydration states, which correspond to heterogeneous states in which several discrete hydrates coexist.[13]

Figure 8 shows the comparison between the swelling of the interlayer space measured by XRD[11,12] and our measurement of the swelling of thin films with Na^{+} or Ca^{2+} interlayer cations by ESEM (already displayed in Figure 5). The swellings of the interlayer space were computed from the data displayed in Figure 1 of the Supporting Information with the engineering definition of strain $\varepsilon = (d/d_{ref}) - 1$, where ε is the swelling, d the interlayer spacing, and d_{ref} the reference interlayer spacing, chosen as the interlayer spacing at maximum relative humidity for each experiment. This choice is consistent with the definition of strain used in our own DIC measurements using the state at a relative humidity equal to 94.8% as the reference state.

For each cation the amplitudes of the swelling between RH = 14% and 95% were identical for the interlayer space and for the film. The convexities of the swelling curves were also identical: convex for the Na^{+}-saturated samples, except at high relative humidities, and concave for the Ca^{2+}-saturated samples. However, the match between the swellings of the interlayer space and of the film was not perfect. Indeed, the XRD experiments measured only the swelling of the clay layers which are perfectly aligned with each others while our ESEM experiment measured the swelling of an ensemble of clay layers, no matter what their orientation was.

4.2. Comparison with Available Data on Adsorbed Amount of Water. Figure 9 displays the comparison between the amount of water adsorbed in the interlayer spaces and the amount adsorbed in the thin films for Na^{+}-saturated montmorillonite (Figure 9a) and for Ca^{2+}-saturated montmorillonite (Figure 9b).

The quantity of water adsorbed in the interlayer space was computed from the XRD data of Bérend et al.[11] and Cases et al.[12] (see Supporting Information) combined with molecular simulations results. The XRD data provided the interlayer

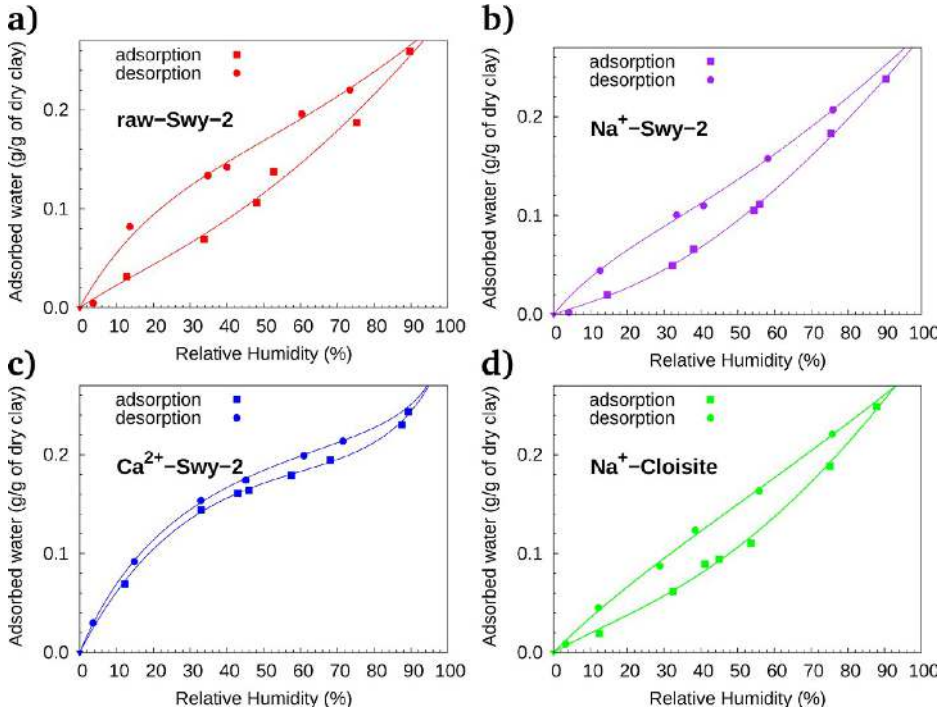

Figure 7. Sorption−desorption isotherms at 20 °C. The solid lines are the fitted curves by the D'Arcy−Watt equation. (a) Natural montmorillonite raw-Swy-2. (b) Na^+-saturated montmorillonite Na^+-Swy-2. (c) Ca^{2+}-saturated montmorillonite Ca^{2+}-Swy-2. (d) Na^+-saturated montmorillonite Na^+-Cloisite. The mass of the dry clays was measured after a 4 h long drying at 110 °C.

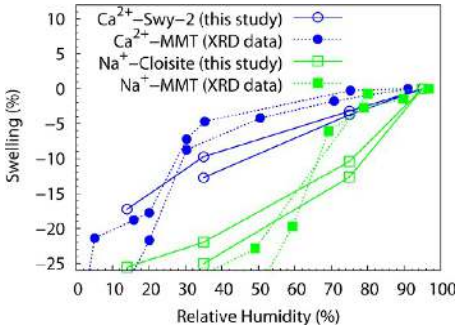

Figure 8. Comparison of the swelling/shrinkage potential of the interlayer space (dashed lines) and of the clay films (solid lines) as a function of relative humidity. The interlayer swelling (Na^+-MMT and Ca^{2+}-MMT curves) was computed from the measurement of the basal spacing by XRD.[11,12] The clay film swelling (Na^+-Cloisite and Ca^{2+}-Swy-2 curves) was our measurement obtained by combining ESEM with DIC. The reference state (0% swelling) was chosen at the maximum relative humidity of each experiment (between 92% and 95%). Round symbols correspond to a Ca^{2+}-saturated montmorillonite, while squared symbols correspond to a Na^+-saturated montmorillonite.

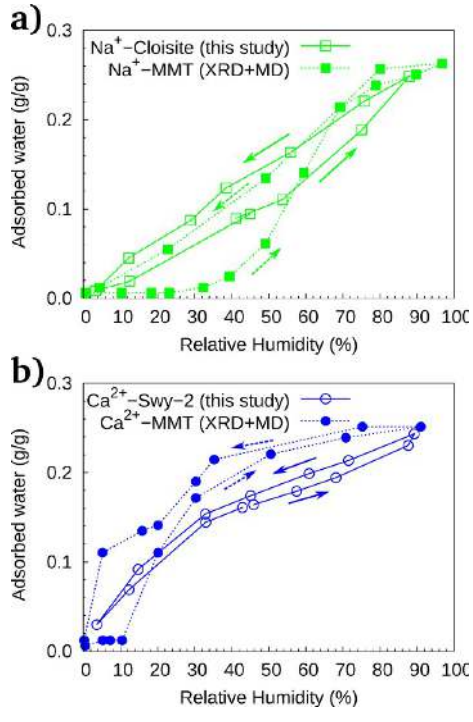

Figure 9. Comparison of the quantity of water adsorbed in the interlayer space (dashed lines) and in clay films (solid lines) as a function of relative humidity. The quantity of water in the interlayer space (Na^+-MMT and Ca^{2+}-MMT curves) was computed from the basal spacing measured by XRD[11,12] combined with results obtained by molecular dynamics simulations. The quantity of water in the clay films (Na^+-Cloisite and Ca^{2+}-Swy-2 curves) was our experimental measurement of the adsorption/desorption isotherms (already displayed in Figure 7). (a) Na^+-saturated montmorillonite. (b) Ca^{2+}-saturated montmorillonite.

spacing in function of relative humidity. We performed the molecular simulations that provided the interlayer spacing in function of the amount of water adsorbed. To do so, we used the atomic structure of a montmorillonite clay layer and the CLAYFF force field and performed molecular dynamics by using the same methodology as Cygan et al.[36] used for a Na^+-montmorillonite. We thus computed the swelling of both Na^+-montmorillonite and Ca^{2+}-montmorillonite. Figure 2 of the Supporting Information displays the results of an isobaric−isothermal (NPT ensemble) molecular dynamics simulation for the two interlayer cations at 300 K and 1 bar. The two curves

differ at low water content because of the different hydration properties of the cations. In contrast, the basal spacings are identical at larger amounts of water and are linear functions of the water content at high relative humidities. With these two sets of data (i.e., XRD and molecular simulation), we could compute the amount of water adsorbed in the interlayer space in function of relative humidity. The adsorption isotherms of the thin films are our experimental measurement of the quantity of water (already displayed in Figure 7).

For each cation, the quantity adsorbed in the film at RH = 90% was close to the quantity adsorbed in the interlayer space. Like for the swelling curves, the adsorption isotherms of the film and of the interlayer space exhibited identical convexity. For the Ca^{2+}-saturated montmorillonite, both the film and the interlayer space adsorbed most water at relative humidities smaller than 45%. In contrast, for the Na^{+}-saturated montmorillonite, both the film and interlayer space adsorbed most water at relative humidities above 45%. Moreover, for both Na^{+}- and Ca^{2+}-saturated samples, the amplitude of the hysteresis for the interlayer space was the same as for the film: this hysteresis was low for the Ca^{2+}-montmorillonite (except at a relative humidity of 10%) while it was high for the Na^{+}-montmorillonite (except at a relative humidity of 80%).

The comparison of the swelling and the adsorption isotherms of the films with available data on the behavior of the interlayer space upon hydration and dehydration showed that the swelling of the clay films was driven principally by the interlayer crystalline swelling. This result is somewhat surprising, in the sense that mesopore swelling usually contributes significantly to the overall swelling of natural clay-based materials, for instance above a relative humidity of 60% for Na^{+}-montmorillonite.[6] A tentative explanation for such surprising result is developed in the next section.

4.3. Pore Structure and Order in Clay Films. At a relative humidity of 35%, the Ca^{2+}-Swy-2 film displayed in Figure 1c was about 35 μm thick upon dehydration. The measured surface density of dry clay of the sample was about 5.6 mg/cm^2 while the surface density of a dry clay layer computed from its structural formula was about 0.27 μg/cm^2: therefore, about 21 000 layers lay in the thickness of the film. At a relative humidity of 35%, upon dehydration, the basal spacing of Ca^{2+}-montmorillonite was 14.8 Å, as shown in Figure 1 of the Supporting Information. The total thickness of a stacking of 21 000 Ca^{2+}-montmorillonite layers under these conditions was 31.1 μm. The mesoporosity, i.e., the fraction of the volume of the sample which was not occupied by the layers and the interlayer spaces, was equal to about 11%. For the Na^{+}-Cloisite displayed in Figure 1d, at a relative humidity of 35%, upon dehydration, the thickness of the film was about 50 μm. The data of Figure 1 of the Supporting Information show that the basal spacing was about 12.5 Å upon dehydration. The measured density of dry clay of the film was 9.6 mg/cm^2. Hence, about 35 000 layers lay in the thickness of the film, and the total thickness of the stacking of all these layers was about 43.8 μm upon dehydration at a relative humidity of 35%. Therefore, the mesoporosity was equal to about 12%. Thus, both the Na^{+}-saturated sample and the Ca^{2+}-saturated sample exhibited the same mesoporosity, slightly larger than 10%. Sammartino et al.[37] estimated that the mesoporosity of argillite occupies 86% of the total porosity. The porosity of a typical argillite is equal to 18%, and the clay matrix fraction is smaller than 50%.[22] Therefore, the mesoporosity of the clay matrix of argillite is larger than 31%. Thus, the mesoporosity of our clay films was at least three times as small as the mesoporosity of a natural isotropic clay matrix.

No or little mesopore swelling took place in contrast to what is observed in disordered macroscopic samples.[6] Therefore, the presence of a small amount of mesoporosity did not contribute to the swelling of the specimen. The clay films did not undergo the very high swellings observed by ESEM on aggregates at relative humidities above 75%,[19] which has also been observed recently at the local scale in clay rocks.[22] In contrast, like for individual clay layers, the clay films displayed significant swelling even at relative humidities below 50%, while such a swelling at low relative humidity is not observed in regular macroscopic clay-based samples.[19,22] A reason why the swelling of our films was similar to that of individual layers, while that of macroscopic samples is not, can be found in the order of the systems considered. Figure 10 shows the difference of structure between a well-ordered clay film and an isotropic natural clay sample: in a disordered clay sample, the swelling of the layers, which occurs mostly orthogonally to the clay particles, is constrained by other particles and the material undergoes significant residual stresses. When mineral inclusions are present in the clay matrix, the constraints on the swelling are even larger and generate strong local strain heterogeneities, as observed by Wang.[22] In contrast, in an ordered clay film, the swelling of a clay particle is much closer to a free swelling. The swelling of each layer is not affected by the neighboring layer.

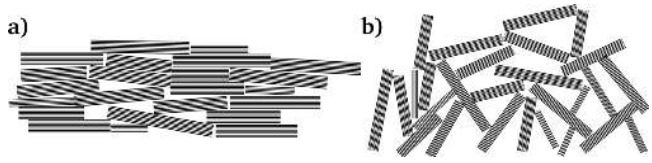

Figure 10. Schematic structure of (a) an ordered clay film, in which the particle orientation is strongly anisotropic, and of (b) a disordered clay sample, in which the particle orientation is less anisotropic.

5. CONCLUSION

The use of environmental scanning electron microscopy allowed us to observe the humidity-induced (for relative humidities between 14% and 95%) of oriented Na^{+}-, Ca^{2+}-, or mixed ("raw") Na^{+},Ca^{2+}-montmorillonite films. Digital image correlation made it possible to quantitatively measure the in-plane and out-of-plane swelling and shrinkage of the self-standing films, with submicrometer accuracy. In parallel, the water adsorption isotherms on similar films were measured and also calculated using molecular dynamics simulations based on previously published X-ray diffraction data. Two key results were obtained. The first one is that the out-of-plane dimensional variations are always more than 1 order of magnitude larger than the in-plane dimensional variations. The second one is that, in the relative humidity range explored in this work, the out-of-plane macroscopic dimensional variations and the associated variations in the amount of adsorbed water can be quasi-entirely accounted for by the subnanometer variations in basal spacing. Both results point to a high orientation and stacking order in the films. Everything happens as if, to a large extent, the films were perfect and freely swelling macroscopic stacks of clay layers, with no significant water-filled void space outside the interlayer space, which could be the source of additional hydromechanical efforts.

This conclusion applies to both Na^+- and Ca^{2+}-exchanged clays, in spite of significant differences in the adsorption isotherms and in the swelling−shrinkage curves. This is surprising at first sight because homoionic montmorillonites exchanged with divalent cations (Ca^{2+} or Mg^{2+}) are known to form tactoids with a rather large number n_l of hydrated layers (average $n_l \geq 4$, up to 20) per tactoid, even in very dilute suspension at low ionic strength, whereas the tactoids formed by montmorillonites exchanged by monovalent cations (Li^+ or Na^+) are essentially individual layers.[8] Hence, our result shows that the formation of tactoids in the parent suspensions used to cast the films does not affect the freely swelling character of the films. Na^+-montmorillonite films behave as well ordered and freely swelling stacks of quasi-individual layers whereas the Ca^{2+}-montmorillonite films behave as well ordered and freely swelling stack of thicker particles, without any significant difference between interlayer swelling and interparticular swelling. However, this conclusion should be taken with caution and restricted to the water activity domain in which the study was performed (relative humidities between 14% and 95%) and in which the swelling mechanism is the so-called crystalline swelling, driven by the hydration of the cations and the surface oxygen atoms. It will most probably break down at larger water activity, in conditions where the osmotic swelling mechanism takes over. In those conditions, the homogeneous interlayer swelling of the Na^+-saturated film would still go on, whereas the interlayer swelling of the Ca^{2+}-saturated film would be severely restricted by ion−ion correlation forces.[38,39]

The next step in the study of highly oriented smectite deposits is to investigate the consequences of their free swelling character on their mechanical properties. Performing mechanical testing on these clay films will make it possible to better characterize the impact of water adsorption in the interlayer space on the mesoscopic mechanical properties. Indeed, the impact of water adsorption in the interlayer space on the mechanical properties at the scale of the engineer needs to be further investigated because it is crucial to many applications in civil and oil and gas engineering. But such impact, although well characterized at the macroscopic scale of the heterogeneous clay-based natural materials, has in contrast not been well characterized at the smaller scales. Here, our model material makes it possible to fill that gap: the manufactured clay films can be pulled with regular mechanical equipments, while ordering in those films enables to ensure that mechanical solicitation is applied in specific directions with respect to the clay layers.

AUTHOR INFORMATION

Corresponding Author

*E-mail matthieu.vandamme@enpc.fr (M.V.).

Notes

The authors declare no competing financial interest.

ACKNOWLEDGMENTS

The environmental scanning electron microscope FEI Quanta 600 used in this study has been acquired with the financial support of Region Île de France (SESAME 2004 program), CNRS, and École Polytechnique.

REFERENCES

(1) Jones, D. E. J.; Holtz, W. G. Expansive soils - The hidden disaster. *Civil Eng.* **1973**, *43*, 49−51.

(2) Anderson, R.; Ratcliffe, I.; Greenwell, H.; Williams, P.; Cliffe, S.; Coveney, P. Clay swelling − A challenge in the oilfield. *Earth-Sci. Rev.* **2010**, *98*, 201−216.

(3) Delage, P.; Cui, Y. J.; Tang, A. M. Clays in radioactive waste disposal. *J. Rock Mech. Geotech. Eng.* **2010**, *2*, 111−123.

(4) Mooney, R. W.; Keenan, A. G.; Wood, L. A. Adsorption of water vapor by montmorillonite. II. Effect of exchangeable cations and lattice swelling as measured by X-ray diffraction. *J. Am. Chem. Soc.* **1952**, *74*, 1371−1374.

(5) Push, R.; Yong, R. N. *Microstructure of Smectite Clays and Engineering Performance*; Taylor & Francis: New York, 2006.

(6) Salles, F.; Bildstein, O.; Douillard, J. M.; Jullien, M.; Raynal, J.; Van Damme, H. On the cation dependence of interlamellar and interparticular water and swelling in smectite clays. *Langmuir* **2010**, *26*, 5028−37.

(7) Shomer, I.; Mingelgrin, U. A direct procedure for determining the number of plates in tactoids of smectites: the Na/Ca-montmorillonite case. *Clays Clay Miner.* **1978**, *26*, 135−138.

(8) Schramm, L. L.; Kwak, J. A. N. C. T. Influence of exchangeable cation composition on the size and shape of montmorillonite particles in dilute suspension. *Clays Clay Miner.* **1982**, *30*, 40−48.

(9) Saiyouri, N.; Tessier, D.; Hicher, P. Experimental study of swelling in unsaturated compacted clays. *Clay Miner.* **2004**, *39*, 469−479.

(10) Laird, D. a. Influence of layer charge on swelling of smectites. *Appl. Clay Sci.* **2006**, *34*, 74−87.

(11) Bérend, I.; Cases, J.-M.; François, M.; Uriot, J.-P.; Michot, L. J.; Masion, A.; Thomas, F. Mechanism of adsorption and desorption of water vapor by homoionic montmorillonites: 2. The Li^+, Na^+, K^+, Rb^+ and Cs^+-exchanged forms. *Clays Clay Miner.* **1995**, *43*, 324−336.

(12) Cases, J.-M.; Bérend, I.; François, M.; Uriot, J.; Michot, L. J.; Thomas, F. Mechanism of adsorption and desorption of water vapor by homoinic montmorillonite: 3. The Mg^{2+}, Ca^{2+}, Sr^{2+}, and Ba^{2+} exchanged forms. *Clays Clay Miner.* **1997**, *45*, 8−22.

(13) Ferrage, E.; Lanson, B.; Sakharov, B. A.; Drits, V. A. Investigation of smectite hydration properties by modeling experimental X-ray diffraction patterns: Part I. Montmorillonite hydration properties. *Am. Mineral.* **2005**, *90*, 1358−1374.

(14) Karaborni, S.; Smit, B.; Heidug, W.; Urai, J.; van Oort, E. The swelling of clays: Molecular simulations of the hydration of montmorillonite. *Science* **1996**, *271*, 1102−1104.

(15) Hensen, E. J. M.; Smit, B. Why clays swell. *J. Phys. Chem. B* **2002**, *106*, 12664−12667.

(16) Tambach, T. J.; Hensen, E. J. M.; Smit, B. Molecular simulations of swelling clay minerals. *J. Phys. Chem. B* **2004**, *108*, 7586−7596.

(17) Romero, E.; Simms, P. H. Microstructure investigation in unsaturated soils: A review with special attention to contribution of mercury intrusion porosimetry and environmental scanning electron microscopy. *Geotech. Geol. Eng.* **2008**, *26*, 705−727.

(18) Montes-H, G. Swelling-shrinkage measurements of bentonite using coupled environmental scanning electron microscopy and digital image analysis. *J. Colloid Interface Sci.* **2005**, *284*, 271−7.

(19) Montes-H, G.; Duplay, J.; Martinez, L.; Geraud, Y.; Rousset-Tournier, B. Influence of interlayer cations on the water sorption and swelling-shrinkage of MX80 bentonite. *Appl. Clay Sci.* **2003**, *23*, 309−321.

(20) Montes-H, G.; Geraud, Y.; Duplay, J.; Reuschle, T. ESEM observations of compacted bentonite submitted to hydration/dehydration conditions. *Colloids Surf., A* **2005**, *262*, 14−22.

(21) Maison, T. Analyse à l'échelle microscopique des phénomènes d'humectation et de dessication des argiles. Ph.D. thesis, École centrale Paris, 2011.

(22) Wang, L. Micromechanical experimental investigation and modelling of strain and damage of argillaceous rocks under combined hydric and mechanical loads. Ph.D. thesis, École Polytechnique, 2012.

(23) Wang, L.; Bornert, M.; Chanchole, S.; Heripre, E. Experimental investigation of the free swelling of crushed argillite. *Geotech. Lett.* **2013**.
(24) Wang, L.; Bornert, M.; Chanchole, S.; Yang, D.; Heripre, E.; Tanguy, A.; Caldemaison, D. Micro-scale experimental investigation of the swelling anisotropy of the Callovo-Oxfordian argillaceous rock. *Clay Miner.* **2013**, *48*, 391−402.
(25) Sutton, M. A.; Schreier, H.; Orteu, J.-J. *Image Correlation for Shape, Motion and Deformation Measurements*; Springer: Boston, MA, 2009.
(26) Zabat, M. Microtexture et propriétés mécaniques de films solides de particules colloïdales. Ph.D. thesis, Université d'Orléans, 1996.
(27) Costanzo, P.; Guggenheim, S. Baseline studies of the Clay Minerals Society source clays: Preface. *Clays Clay Miner.* **2001**, *49*, 371−371.
(28) Mermut, A. R.; Faz Cano, A. Baseline studies of the Clay Minerals Society source clays: Chemical analyses of major elements. *Clays Clay Miner.* **2001**, *49*, 381−386.
(29) Arroyo, J. L.; Li, H.; Teppen, B. J.; Boyd, S. A. A simple method for partial purification of reference clays. *Clays Clay Miner.* **2005**, *53*, 512−520.
(30) Pospísil, M.; Kalendová, A.; Capková, P.; Simonk, J.; Valásková, M. Structure analysis of intercalated layer silicates: Combination of molecular simulations and experiment. *J. Colloid Interface Sci.* **2004**, *277*, 154−61.
(31) Dautriat, J.; Bornert, M.; Gland, N.; Dimanov, A.; Raphanel, J.; Vizika, O. Micromechanical investigation of the hydromechanical behaviors of carbonates contribution of in-situ strain field measurement by means of SEM and optic digital image correlation. *Petrophysics* **2010**, *51*, 388−398.
(32) Allais, L.; Bornert, M.; Bretheau, T.; Caldemaison, D. Experimental characterization of the local strain field in a heterogeneous elastoplastic material. *Acta Metall. Mater.* **1994**, *42*, 3865−3880.
(33) Bornert, M.; Valès, F.; Gharbi, H.; Nguyen Minh, D. Multiscale full-field strain measurements for micromechanical investigations of the hydromechanical behaviour of clayey rocks. *Strain* **2010**, *46*, 33−46.
(34) Bornert, M.; Brémand, F.; Doumalin, P.; Dupré, J.-C.; Fazzini, M.; Grédiac, M.; Hild, F.; Mistou, S.; Molimard, J.; Orteu, J.-J.; Robert, L.; Surrel, Y.; Vacher, P.; Wattrisse, B. Assessment of digital image correlation measurement errors: Methodology and results. *Exp. Mech.* **2008**, *49*, 353−370.
(35) D'Arcy, R. L.; Watt, I. C. Analysis of sorption isotherms of non-homogeneous sorbents. *Trans. Faraday Soc.* **1970**, *66*, 1236−1245.
(36) Cygan, R. T.; Liang, J.-J.; Kalinichev, A. G. Molecular models of hydroxide, oxyhydroxide, and clay phases and the development of a general force field. *J. Phys. Chem. B* **2004**, *108*, 1255−1266.
(37) Sammartino, S.; Bouchet, a.; Prêt, D.; Parneix, J.-C.; Tevissen, E. Spatial distribution of porosity and minerals in clay rocks from the Callovo-Oxfordian formation (Meuse/Haute-Marne, Eastern France)-implications on ionic species diffusion and rock sorption capability. *Appl. Clay Sci.* **2003**, *23*, 157−166.
(38) Kjellander, R.; Mareelja, S.; Pashley, R. M.; Quirk, J. P. Double-layer ion correlation forces restrict calcium-clay swelling. *J. Petrol. Sci. Eng.* **1988**, *92*, 6489−6492.
(39) Kjellander, R.; Marcelja, S.; Quirk, J. P. Attractive double-sayer interactions between calcium clay particles. *J. Colloid Interface Sci.* **1988**, *126*, 194−211.